A FAST NON-PARAMETRIC ALGORITHM FOR COHERENT CHANGE DETECTION

Giovanni Costa, Andrea Monti Guarnieri, Marco Manzoni

Alessandro Parizzi

Politecnico di Milano
DEIB
Via G. Ponzio, 34, 20133, Milano MI

TRE ALTAMIRA s.r.l.
Ripa di Porta Ticinese 79, 20143
Milan, Italy

ABSTRACT

Developing algorithms to detect temporal and spatial changes in radar targets is paramount. This paper specifically addresses the temporal change detection aspect, introducing a rapid non-parametric Coherent Change Detection (CCD) algorithm named Fast-Permutational Change Detection (F-PCD). The F-PCD identifies temporal Change Points (CPs) in a radar target by recognizing *block structures* in the coherence matrix, showing great robustness against non-stationary noise sources that generally affect the performance of the standard approaches. Moreover, the F-PCD is characterized by an accelerated inference process, ensuring efficiency without substantial performance loss. The F-PCD algorithm can be applied to different scenarios, for example, where DEM changes happen, e.g., mining sites, volcano eruptions, and earthquakes. For this reason, an example of the F-PCD application on an active open-pit mining site is presented to validate its effectiveness. Moreover, its generalization capability is demonstrated by a multi frequency-geometry analysis conducted on the same mining site. Finally, fully exploiting the F-PCD outcomes contributes to a broader understanding of temporal changes in SAR data and introduces new perspectives for interpreting InSAR datasets.

Index Terms— SAR, Coherent Change Detection, Permutation Tests, Object Counter, Open Pit Mine

1. INTRODUCTION

Over the past two decades, Synthetic Aperture Radar (SAR) has proven highly effective in studying surface deformation phenomena (InSAR). Radar targets can be point-wise or PS [1] widely available in urban areas but also distributed DS [2][3], present mainly in non-urban areas. Current algorithms face challenges adapting to changes in the analyzed scenario. Whether PS or DS can evolve, potentially disappearing, while new measurement points may emerge. The proposed method, called Fast-Permutational Change Detection (F-PCD), operates within the Coherent Change Detection (CCD) [4] [5] [6] [7] framework, aiming to detect significant temporal changes that manifest as block structures in the coherence matrix of

the radar target. It does so rapidly, flexibly, and straightforwardly, exhibiting great robustness even in the presence of non-stationary noise sources. The algorithm's intricacies are expounded in Section 2 following a theoretical introduction to the coherence matrix and permutation tests. Subsequently, in Section 3, the F-PCD is compared with the GLRT algorithm presented in [7] and then applied to real data in an active open-pit mine area, chosen for its rapid environmental changes. Finally, a multi frequency-geometry analysis is performed on the same area of interest to validate the algorithm and to show its generalization capability.

2. FAST-PERMUTATIONAL CHANGE DETECTION

The *Fast-Permutational Change Detection* (F-PCD) [8] is a non-parametric CCD algorithm that estimates changes in coherence of a radar target and block structure in the coherence matrix $\hat{\Gamma}$. It consists of a single step, the *Permutational Screener*, which contemporary detects and validates the change points (CPs). The output is the *Change Detection Matrix* (CDM) detailed in the Sub-Section 2.2. For a more comprehensive grasp of the mathematical intricacies, the Sub-Section 2.1 provides an overview of the most crucial theoretical concepts.

2.1. Coherence Matrix and Permutation Tests

2.1.1. Coherence Matrix

Given a SAR data stack of NI images, $\hat{\Gamma}$ is the $[NI, NI]$ matrix containing the modulus of the interferometric coherence $\hat{\gamma}_{ij}$ between the i_{th} and j_{th} image, estimated over a window of dimension L number of looks. By following [9] [10] [11] [12] [13] [14], it can be approximated as

$$\hat{\Gamma} \simeq \gamma_0 \gamma_t \gamma_b \gamma_n, \tag{1}$$

where

- γ_0: maximum theoretical coherence, the value of the coherence under ideal conditions;

- $\gamma_t = e^{-\frac{|B_{t_{ij}}|}{\tau}}$: temporal decorrelation with time constant τ [13];

- $\gamma_b = \left(1 - \frac{B_{n_{ij}}}{B_c}\right)$: geometrical decorrelation with B_c critical baseline [15];

- γ_n: decorrelation due to other noise sources.

Whenever a radar target undergoes an abrupt change, $\hat{\Gamma}$ presents *blocks structure*, implying that the change is not reversible. Mathematically, a block $\mathcal{B}$ is a submatrix of $\hat{\Gamma}$ determined by a group of consecutive coherence estimates much greater than the ones outside the block. Being

$$\mathcal{D} = \{1, 2, ..., NI\},$$

the set of the observations' indexes, $\mathbf{y}(l) \in \mathbb{C}^{NI}$ the vector collecting the temporal samples of the l-th pixel, and

$$\mathcal{I} = \left\{k \in \mathcal{D} \,\Big|\, \frac{1}{L}\left|\sum_{l=1}^{L} y_k(l) y_h^{\,H}(l)\right| > \epsilon \,\forall h \in \mathcal{D} \text{ and } h \neq k\right\},$$

the groups of observations' indexes satisfying the condition above, then a block $\mathcal{B}$ is

$$\mathcal{B} = \{\hat{\gamma}_{ij} \in \hat{\Gamma} \,|\, i, j \in \mathcal{I}\}. \tag{2}$$

Then, it is possible to write the $ij - th$ element of $\hat{\Gamma}$ as

$$\hat{\gamma}_{ij} \simeq \gamma_{\mathcal{B}_{ij}} \gamma_{t_{ij}} \gamma_{b_{ij}} \gamma_{n_{ij}}, \tag{3}$$

where $\gamma_{t_{ij}}, \gamma_{b_{ij}}$ and $\gamma_{n_{ij}}$ are respectively the values of the temporal and geometrical decorrelation and of the noise for the given interferometric pair. Instead, $\gamma_{\mathcal{B}_{ij}}$ is the $ij - th$ element of the block model of $\hat{\Gamma}$, which is always zero except for the case when $i, j \in \mathcal{I}$ where it is equal to one.

2.1.2. Permutation Tests

The permutation test [16], operates on a straightforward principle. Given two statistical populations, A and B, of any size, the test aims to assess a hypothesis $\mathcal{H}_0$ or $\mathcal{H}_1$, achieved by defining a test statistic $T(X)$ and estimating the $p-value(\hat{p})$. The estimation involves repeating $\mathcal{P}$ times the measurement $T(X)$ over new populations $\tilde{A}$ and $\tilde{B}$ with the same cardinalities as the original ones, randomly sampled from the combined ensemble [17]. Then $\hat{p}$ is expressed as

$$\hat{p} = \frac{\#(T^* > T_0)}{\mathcal{P}}, \tag{4}$$

where T_0 is the value of $T(X)$ over the original population. The transformation must preserve any relationships among the populations, to ensure the exactness of the test. In the end, the significance test affirms H_0 with a significance level α if $\hat{p} < \alpha$, where α can be fixed at a specific value [17].

2.1.3. Permutational Screener

The Permutational Screener constitutes a fully permutational step, where the populations under examination are directly derived from the exploitation of the double dimension of $\hat{\Gamma}$. The approach involves opening a squared window with an initial size w_m along the main diagonal and progressively comparing the statistical population inside it, i.e., candidate $\mathcal{B}$, with the corresponding candidate noise block $\mathcal{N} = \mathcal{B}^c$. The initial size w_m is iteratively increased by a factor of one until a change point is identified. Then, it is re-initialized commencing from the next line. A critical consideration is the wise selection of $\mathcal{P}$, which depends on the cardinality of the populations. Assume to have a $\hat{\Gamma}_{[NI,NI]}$, and assume to measure the cardinalities of the populations from a generic index i and with a window size $w > w_m$, then

$$\mathcal{N} = \hat{\Gamma}(i : i+w, i+w+1 : NI) \implies \#\mathcal{N} = (NI-i-w)w, \tag{5}$$

and

$$\mathcal{B} = \hat{\Gamma}(i : i+w, i : i+w) \implies \#\mathcal{B} = \frac{w(w-1)}{2}. \tag{6}$$

In this scenario $\mathcal{P}$ is is entirely uncontrollable, in fact

$$\mathcal{P} \propto \mathcal{P}_{tot} = \binom{\#\mathcal{B} + \#\mathcal{N}}{\#\mathcal{N}} = f(w, NI, i), \tag{7}$$

that implies the impossibility of uniquely limiting them. The suggested solution involves reducing the coherence observation bandwidth B_w, i.e., represent $\hat{\Gamma}$ through a smaller set of $\hat{\gamma}_{ij}$ values. In formulas, considering $\hat{\gamma}_i$ as the generic $i - th$ row $\hat{\Gamma}$, it follows (8)

$$\hat{\gamma}_i = \begin{cases} \hat{\gamma}_{ij} & \text{if } i - B_w < j < i + B_w, \\ 0 & \text{otherwise.} \end{cases} \tag{8}$$

Then, making sure that $BW \geq w_m$, Equation (5) becomes (9)

$$\mathcal{N} = \hat{\Gamma}(i : w^{(i)}, w^{(i)}+1 : w^{(i)}+B_w) \implies \#\mathcal{N} = (B_w-1)w, \tag{9}$$

where $w^{(i)} = i + w$ for compactness. Because only a few elements of $\mathcal{N}$ are non-zero (8), and by enforcing $\#\mathcal{B} = \#\mathcal{N}$ with the selection the last unique $\#\mathcal{N}$ samples of $\mathcal{B}$, Equation (7) can be simplified as (10)

$$\mathcal{P} \propto \mathcal{P}_{tot} = \binom{2\#\mathcal{N}}{\#\mathcal{N}} = f(B_w). \tag{10}$$

In this way, the F-PCD directs its attention towards the transitions between adjacent blocks within the matrix.
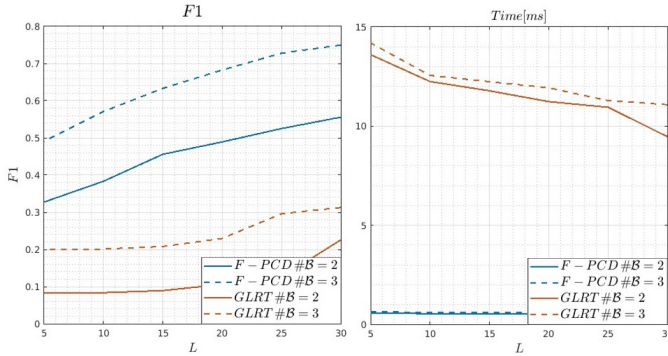
The proposed test statistic $T(X)$ to measure the statistical distance between the two populations is

$$T(X) = \frac{\text{med}(\mathcal{B})}{\sigma_{\mathcal{B}}^2} - \frac{\text{med}(\mathcal{N})}{\sigma_{\mathcal{N}}^2}, \tag{11}$$

the weighted difference of the medians of the populations.

Table 1: Simulation Parameters.

t_r [days]	τ [days]	B_n [m]	B_c [m]	B_w	L	$\#\mathcal{B}$	NI
12	90	[-200, 200]	1300	4	5, ...,30	2,3	30

Fig. 1: Performance comparison between F-PCD and GLRT in terms of F1-score (left) and computational time (right).

2.2. F-PCD Outputs

The F-PCD produces as output the *Change Detection Matrix* (CDM), an $[NI, NI]$ matrix showing the estimated block model for $\hat{\Gamma}$. It is filled following these rules:

- Assigns 0.5 to all the rows whose maximum in $\hat{\Gamma}$ is below the noise threshold th_n [8] (*bad images*);

- Whenever a CP is detected, fill the corresponding block $\mathcal{B}$ with 1.

3. RESULTS FROM SIMULATED AND REAL DATA

The algorithm is firstly compared with the GLRT approach [7], in terms of computational time and their F1-score [18]. The performance has been measured on synthetic data out of 5000 Monte Carlo simulations assuming blocks of equal extension. The settings are shown in Table 1. As anticipated, a thorough examination of Figure 1 reveals that the F-PCD outperforms the GLRT, especially under conditions of a low number of looks. The improvement in performance for the GLRT algorithm is noticeable only when $\#\mathcal{B} = 2$. This indicates that in highly dynamic environments, the F-PCD may be the preferred choice, as indicated by the performance curve for $\#\mathcal{B} = 3$. Regarding computational time, the F-PCD is faster than the GLRT and is less influenced by the number of looks. Shifting to real-world data, the chosen case study is an open-pit mine area due to the rapid and dynamic environmental changes. The dataset comprises the descending track 20 TerraSAR-X, SL 037 mode, and VV polarization. The temporal interval spans from January 2022 to December 2022,
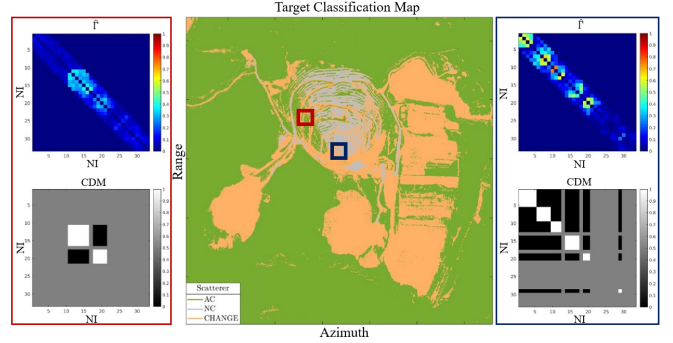
Fig. 2: Examples of F-PCD result over an open-pit mine area. In the center is the Target Classification, and on the left and right are examples of CDM, respectively taken from the roads inside the pit (red) and the bottom part of the pit (blue).

consisting of 33 images acquired every 11 days, with only one missing acquisition. For this analysis, B_w is set equal to four, resulting in a reduction of $\mathcal{P}$ to 10. It is possible to demonstrate that this value represents the minimum number of permutations, ensuring that RMSE affecting $\hat{p}$ remains within acceptable limits, still guaranteeing overall good performance. Figure 2 illustrates examples of CDM generated by the algorithm and the target classification map, where the targets are labeled as *Always Coherent* (AC), *Never Coherent* (NC), or changed (CHANGE). As it is possible to note, the F-PCD shows great robustness against non-stationary noise sources. This feature can be appreciated by the inspection of the second block detected in the red case example in Figure 2, as well as the fourth of the blue one: for both cases, the detection is challenging because of the presence of randomly decorrelated pairs, which generally imply false alarms in standard approaches. The F-PCD can correctly handle this kind of case by directly inspecting the data and building statistics on the observable (Sub-Section 2.1.3). Generating general CD maps is somewhat restrictive when contemplating the algorithm's full potential. The F-PCD outputs offer a more comprehensive understanding of the nature of radar scatterers within the Area of Interest (AOI). By utilizing the pixel-wise information in the CDM, a thorough interpretation of the entire scene, encompassing targets unaffected by changes, becomes achievable. As illustrated in Figure 3, this more detailed interpretation can be addressed by associating each pixel with the corresponding number of objects defined in relation to the block structure (Sub-Section 2.1) and including the information about the number of changes and the number of bad images associated with each pixel. Finally, the F-PCD has been applied in the same area and during the same time frame on the data collected by the TerraSAR-X ascending SM005 track 134 and the ascending track 47 of Sentinel-1 IW, both in VV polarization. The results of the three different analyses have been then intersected on a common georeferenced grid, and the changed areas have been dated based on the three different
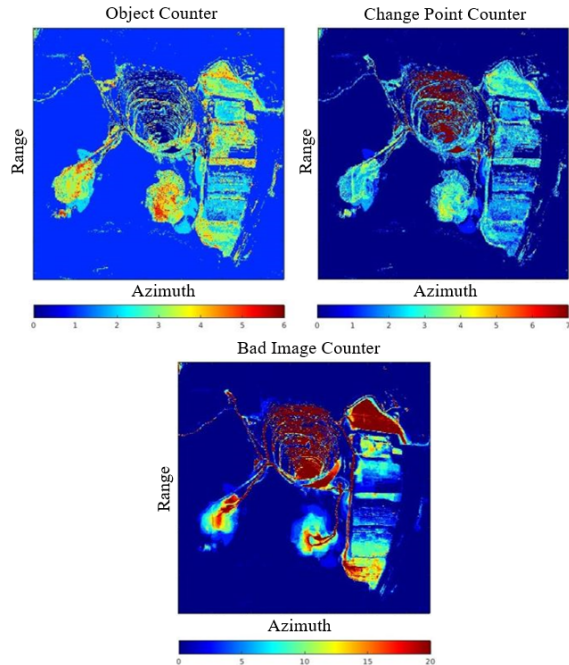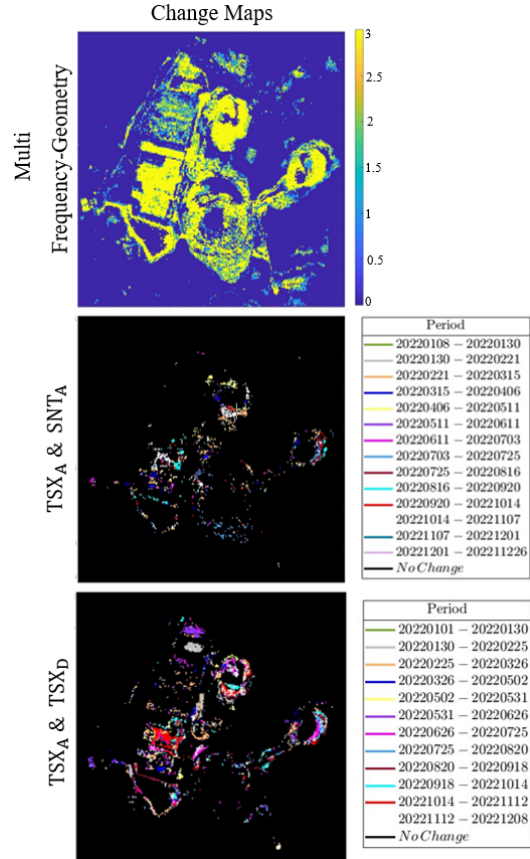
Fig. 3: The Object Counter, the Change Point Counter, and the Bad Image counter in SAR coordinates, respectively, on the top left, top right, and bottom, of the descending track 20 TerraSAR-X.

Fig. 4: Change Maps from the multi frequency-geometry analysis on a common georeferenced grid. On the top is the map cumulative change map, where the pixel values highlight the number of sensors detecting that change. On the bottom and the center are the intersections of the changes between the TerraSAR-X geometries and the TerraSAR-X Sentinel-1 ascending geometries, with their relative time period.

datasets. The result of the multi frequency-geometry analysis is shown in Figure 4. The multi-frequency-geometry cumulative change map is at the top, reporting the number of sensors highlighting that change for each changed pixel. The changed areas characterized by pixel values of 1 or 2 are affected by geometric distortions, at least in one of the considered geometries. The missing areas are the ones characterized by many *bad images* (Figure 3). Instead, at the center and the bottom are the intersections between the TerraSAR-X Sentinel-1 ascending geometries and the TerraSAR-X geometries. As it is possible to note, the main difference is related to the resolution of the two maps due to the different paired-sensors resolution. However, the colored areas are dating the changes exactly in the same period, allowing users to locate the change in the spatio-temporal framework precisely. These final results not only validate the effectiveness of the proposed method but also definitely highlight its generalization capabilities.

4. CONCLUSIONS

This paper introduces the Fast Permutational Change Detection (F-PCD), whose significant innovation lies in its application without imposing stringent assumptions and without necessitating the modeling of parameters because it moves directly on the data observation; because of this, F-PCD

has proved to be very robust in detecting changes in coherence across various scenarios, even in the presence of non-stationary noise sources. The quantitative comparison with the GLRT algorithm highlights its robustness, especially at a low number of looks, along with a competitive computational time. Furthermore, real data analysis proposes a new perspective for interpreting InSAR datasets. In fact, by leveraging the outputs of F-PCD, it becomes possible to describe each target based on the number of its coherent lives (objects), the number of temporal changes, and the number of noisy acquisitions affecting it. This approach facilitates a direct and intuitive association between possible measurement points and their reliability. Finally, the method has been validated through a multi frequency-geometry analysis, allowing the users to date the changes precisely and highlighting the capabilities of generalization of the F-PCD.

5. REFERENCES

[1] A Ferretti, C Prati, and F Rocca, "Non-uniform motion monitoring using the permanent scatterers technique," *FRINGE'99: Advancing ERS SAR Interferometry from Applications towards Operations*, 2000.

[2] Alessandro Ferretti, Alfio Fumagalli, Fabrizio Novali, Claudio Prati, Fabio Rocca, and Alessio Rucci, "A new algorithm for processing interferometric data-stacks: SqueeSAR," *IEEE Transactions on geoscience and remote sensing*, vol. 49, no. 9, pp. 3460–3470, 2011.

[3] Kanika Goel and Nico Adam, "A distributed scatterer interferometry approach for precision monitoring of known surface deformation phenomena," *IEEE Transactions on Geoscience and Remote Sensing*, vol. 52, no. 9, pp. 5454–5468, 2014.

[4] Jungkyo Jung, Duk-jin Kim, Marco Lavalle, and Sang-Ho Yun, "Coherent change detection using inSAR temporal decorrelation model: A case study for volcanic ash detection," *IEEE Transactions on Geoscience and Remote Sensing*, vol. 54, no. 10, pp. 5765–5775, 2016.

[5] Mark Preiss and Nicholas JS Stacy, "Coherent change detection: Theoretical description and experimental results," Tech. Rep., 2006.

[6] Jungkyo Jung, Duk-jin Kim, Sang-ho Yun, and Marco Lavalle, "Damage mapping based on coherence model using multi-temporal polarimetric-interferometric uavsar data," in *2017 IEEE International Geoscience and Remote Sensing Symposium (IGARSS)*. IEEE, 2017, pp. 189–192.

[7] Andrea Virgilio Monti-Guarnieri, Maria Antonia Brovelli, Marco Manzoni, Mauro Mariotti d'Alessandro, Monia Elisa Molinari, and Daniele Oxoli, "Coherent change detection for multipass SAR," *IEEE Transactions on Geoscience and Remote Sensing*, vol. 56, no. 11, pp. 6811–6822, 2018.

[8] Giovanni Costa, Andrea Virgilio Monti Guarnieri, Marco Manzoni, and Alessio Rucci, "A non-parametric estimator for coherent change detection: the permutational change detection," *IEEE Transactions on geoscience and remote sensing*, Submitted Nov. 2023.

[9] Richard Bamler and Philipp Hartl, "Synthetic aperture radar interferometry," *Inverse problems*, vol. 14, no. 4, pp. R1, 1998.

[10] P.A. Rosen, S. Hensley, I.R. Joughin, F.K. Li, S.N. Madsen, E. Rodriguez, and R.M. Goldstein, "Synthetic aperture radar interferometry," *Proceedings of the IEEE*, vol. 88, no. 3, pp. 333–382, 2000.

[11] Dieter Just and Richard Bamler, "Phase statistics of interferograms with applications to synthetic aperture radar," *Appl. Opt.*, vol. 33, no. 20, pp. 4361–4368, Jul 1994.

[12] Andrea Monti Guarnieri and Stefano Tebaldini, "On the exploitation of target statistics for SAR interferometry applications," *IEEE Transactions on Geoscience and Remote Sensing*, vol. 46, no. 11, pp. 3436–3443, 2008.

[13] Fabio Rocca, "Modeling interferogram stacks," *IEEE Transactions on Geoscience and Remote Sensing*, vol. 45, no. 10, pp. 3289–3299, 2007.

[14] Howard A Zebker, John Villasenor, et al., "Decorrelation in interferometric radar echoes," *IEEE Transactions on geoscience and remote sensing*, vol. 30, no. 5, pp. 950–959, 1992.

[15] Alessandro Ferretti, Andrea Monti-Guarnieri, Claudio Prati, Fabio Rocca, and Didier Massonet, *InSAR principles-guidelines for SAR interferometry processing and interpretation*, vol. 19, 2007.

[16] Ronald A Fisher, "" The coefficient of racial likeness" and the future of craniometry," *The Journal of the Royal Anthropological Institute of Great Britain and Ireland*, vol. 66, pp. 57–63, 1936.

[17] Bruce Brown, "Permutation tests for complex data: Theory, applications and software by F. Pesarin and L. Salmaso," 2012.

[18] Cyril Goutte and Eric Gaussier, "A probabilistic interpretation of precision, recall and f-score, with implication for evaluation," in *European conference on information retrieval*. Springer, 2005, pp. 345–359.